

1 **Characteristics of aerosol pollution during heavy haze events**  
2 **in Suzhou, China**

3

4 **M. Tian<sup>1</sup>, H. B. Wang<sup>1</sup>, Y. Chen<sup>1</sup>, F. M. Yang<sup>1,2,3\*</sup>, X. H. zhang<sup>4</sup>, Q. Zou<sup>4</sup>, R. Q.**  
5 **Zhang<sup>4</sup>, Y. L. Ma<sup>5</sup>, K. B. He<sup>5</sup>**

6 <sup>1</sup>Key Laboratory of Reservoir Aquatic Environment of CAS, Chongqing Institute of  
7 Green and Intelligent Technology, Chinese Academy of Sciences, Chongqing 400714,  
8 China

9 <sup>2</sup>Center for Excellence in Urban Atmospheric Environment, Institute of Urban  
10 Environment, Chinese Academy of Sciences, Xiamen 361021, China

11 <sup>3</sup>Changjiang Normal University, Chongqing 408100, China.

12 <sup>4</sup>Suzhou Environmental Monitoring Center, Suzhou 215004, China

13 <sup>5</sup>School of Environment, Tsinghua University, Beijing 100012, China

14 *Correspondence to:* F. M. Yang (fmyang@cigit.ac.cn)

15

16 **Abstract**

17 Extremely severe haze weather events occurred in many cities in China, especially in  
18 the east part of the country, in January 2013. Comprehensive measurements including  
19 hourly concentrations of PM<sub>2.5</sub> and its major chemical components (water-soluble  
20 inorganic ions, OC, and EC) and related gas-phase precursors were conducted via  
21 on-line monitoring system in Suzhou, a medium size city of Jiangsu province, just  
22 east of Shanghai. PM<sub>2.5</sub> frequently exceeded 150  $\mu\text{g m}^{-3}$  on hazy days, with the  
23 maximum reaching 324  $\mu\text{g m}^{-3}$  on Jan. 14, 2013. Unfavorable weather conditions  
24 (high RH, and low rainfall, wind speed and atmospheric pressure) were conducive for  
25 the haze formation. High concentrations of secondary aerosol species (including SO<sub>4</sub><sup>2-</sup>,  
26 NO<sub>3</sub><sup>-</sup>, NH<sub>4</sub><sup>+</sup>, and SOC) and gaseous precursors were observed during the first two  
27 haze events, while elevated primary carbonaceous species emissions were found  
28 during the third haze period, pointing to different haze formation mechanisms. OM,  
29 (NH<sub>4</sub>)<sub>2</sub>SO<sub>4</sub>, NH<sub>4</sub>NO<sub>3</sub> were found to be the major contributors to visibility impairment.  
30 High concentrations of sulfate and nitrate might be explained by homogeneous  
31 gas-phase reactions under low RH conditions and by heterogeneous processes under  
32 relatively high RH conditions. Analysis of air mass trajectory clustering and potential  
33 source contribution function manifested that aerosol pollutions in the studied areas  
34 were mainly caused by local activities and surrounding sources transported from  
35 nearby cities.

36

37 **1. Introduction**

38 Haze is defined as visibility lower than 10 km when relative humidity < 80%. Rapidly  
39 increased air pollution in China in the past several decades have resulted in frequent  
40 occurrences of haze events, which have caused great concern to the scientific  
41 community as well as the public (Zhang et al., 2012). Haze events have adverse  
42 effects on human health, traffic, climate, and other important aspects (Zhang et al.,  
43 2015; Charlson et al., 1987; Ramanathan and Vogelmann, 1997; Tegen et al., 2000; Yu  
44 et al., 2002; Tie et al., 2009a; Tie et al., 2009b). Fine particles (PM<sub>2.5</sub>, aerosols with an

45 aerodynamic diameter of 2.5 microns or less) are largely responsible for haze  
46 formation due to their ability in light extinction including scattering and absorbing  
47 solar and infrared radiation (Yu et al., 2014). Light extinction of PM<sub>2.5</sub> is highly  
48 associated with its chemical composition (Tao et al., 2014). Water-soluble inorganic  
49 ions and carbonaceous species often account for major fractions of PM<sub>2.5</sub> and are  
50 important contributors to visibility impairment (Tan et al., 2009; Pathak et al., 2009),  
51 and thus have been investigated extensively (Yang et al., 2005; Jansen et al., 2014;  
52 Pathak et al., 2009). Most existing studies were based on filter sampling and off-line  
53 analysis and had limitations in providing detailed insight into the roles the major  
54 chemical species played during shorter haze periods.

55 High contributions of secondary inorganic aerosols (SIA, including sulfate,  
56 nitrate and ammonium), the predominant water-soluble ionic species in PM<sub>2.5</sub>, to  
57 visibility reduction have been observed in many cities in China (Huang et al., 2014).  
58 Gas- or liquid-phase reactions of sulfur dioxide and nitrogen oxides are the primary  
59 mechanisms forming aerosol sulfate and nitrate. For the formation of sulfate,  
60 homogeneous gas phase reaction of SO<sub>2</sub> with OH radical, and heterogeneous reactions  
61 in the aqueous surface layer of pre-existing particles and in-cloud processes are the  
62 primary mechanisms (Wang et al., 2006). The rates of gas-phase and liquid-phase  
63 reactions of SO<sub>2</sub> were similar in summer while the heterogeneous processes were  
64 responsible for the oxidation in winter (Hewitt, 2001). Nitric acid can be formed from  
65 homogeneous gas-phase reactions of NO<sub>2</sub> with OH or O<sub>3</sub> and from heterogeneous  
66 hydrolysis of N<sub>2</sub>O<sub>5</sub>, which occurred predominantly during daytime and nighttime,  
67 respectively (Khoder, 2002). Both sulfuric acid and nitric acid react with alkaline  
68 substance in the atmosphere, mostly ammonia under ambient conditions to produce  
69 salts (Hewitt, 2001). The neutralization of sulfuric acid by ammonia has been found to  
70 be preferred over the formation of ammonium nitrate (Warneck, 1999). Thus, the  
71 formation of ammonium nitrate in fine particles is usually under significantly  
72 neutralized or ammonium-rich conditions (Pathak et al., 2009). There are various  
73 factors influencing the formation of aerosol sulfate and nitrate, such as the levels of

74 gaseous precursors (SO<sub>2</sub>, NH<sub>3</sub>, NO<sub>x</sub>) and oxidants, the characteristics of pre-existing  
75 aerosols, and meteorological conditions. These factors may vary by location, resulting  
76 in different formation mechanism in different areas. For instance, different formation  
77 pathways had been reported for nitrate in ammonia-rich and ammonia-deficient areas  
78 (Pathak et al., 2009).

79 In January 2013, extremely severe, persistent and widespread haze weather  
80 occurred in 10 provinces in central and eastern China. These serious pollution events  
81 not only had great adverse effects on human health, as seen in a sharp increase in  
82 respiratory diseases, but also caused immeasurable economic loss (Huang et al., 2014;  
83 Chen et al., 2013). High secondary inorganic and organic aerosol contributions to  
84 particulate pollution during these haze events were reported in a recent study based on  
85 the measurements at urban sites in Beijing, Shanghai, Guangzhou and Xi'an, which  
86 located in the northern, eastern, southern and western regions of China, respectively  
87 (Huang et al., 2014). In addition to investigating primary particulate emissions, the  
88 formation mechanisms of these secondary species and related affecting factors also  
89 need to be understood in order to controlling PM<sub>2.5</sub> levels in China.

90 The Yangtze River Delta (YRD), the Pearl River Delta,  
91 Beijing–Tianjin–Tangshan, and the Sichuan Basin are the four regions with heaviest  
92 haze influence in China. The characteristics and formation mechanisms of haze in the  
93 YRD are different from other haze regions, such as Beijing and the Pearl River Delta  
94 (Fu et al., 2008). Suzhou is located in the heartland of YRD region and is an important  
95 city. It suffered from the extremely serious aerosol pollution in Jan. 2013. With the  
96 tremendous economic growth over the past 30 years, Suzhou has experienced high  
97 levels of air pollution as reflected in the frequency of haze occurrence. The annual  
98 haze days in Suzhou increased from only two days to more than 150 days from 1956  
99 to 2011, i.e. over 40% of days were hazy in 2011. The low visibility, particularly the  
100 haze, has become a major concern of the city. However, only a few studies have  
101 focused on haze events in Suzhou and little is known about the chemical  
102 characteristics and sources of fine particles in this city. To fill these knowledge gaps,

103 an intensified monitoring campaign was launched from December 2012 to January  
104 2013 to collect high temporal resolution chemical and meteorological data. The  
105 objectives of this study are to (1) identify the dominant species in PM<sub>2.5</sub> and  
106 responsible for the visibility reduction; (2) explore the formation mechanism of the  
107 aerosol pollution; (3) study the impact of local, nearby and remote sources on the  
108 formation of haze in urban Suzhou.

109

## 110 **2. Methodology**

### 111 **2.1 Field observations**

112 The sampling station was set up at the roof of one building in Suzhou Institute of  
113 Environmental Sciences (31°20'N, 120°36'E) (Fig. 1), about 300 m west to Nanyuan  
114 South Road and 360 m north to S Ring Road Elevated Bridge. There is no industrial  
115 source nearby and the site is representative of an urban residential and commercial  
116 environment. Suzhou is located in the center of Yangtze River Delta (YRD) and about  
117 80 km east of Shanghai and 200 km west of Nanjing.

118 On-line hourly PM<sub>2.5</sub> mass concentrations were measured using tapered element  
119 oscillating microbalance (TEOM1405, Thermo Scientific Corp., MA, US) with the  
120 heating temperature of 50 °C. Some of the volatile particulate matter might be lost at  
121 50 °C, but comparisons with collocated filters showed that the loss was less than  
122 10%-20% of the gravimetric mass (Chow et al., 2008).

123 Hourly real-time concentrations of five cations (Na<sup>+</sup>, K<sup>+</sup>, NH<sub>4</sub><sup>+</sup>, Ca<sup>2+</sup>, and Mg<sup>2+</sup>)  
124 and four anions (F<sup>-</sup>, Cl<sup>-</sup>, NO<sub>3</sub><sup>-</sup>, and SO<sub>4</sub><sup>2-</sup>) in PM<sub>2.5</sub> were determined by URG Series  
125 9000 Ambient Ion Monitor (AIM, URG Corporation, Chapel Hill, NC). The system  
126 consists of a particle collection unit and two ion chromatograph analyzers for cation  
127 and anion analyses. PM<sub>2.5</sub> was separated by a sharp-cut cyclone inlet operating at a  
128 flow rate of 3 L/min. The air was drawn through a liquid diffusion parallel-plate  
129 denuder to remove the interfering acidic and basic gases. A Steam-Jet Aerosol

130 Collector was placed downstream of the denuder for collection and extraction of  
131 particles. The water extract was subsequently injected into the two ICs once an hour.  
132 The estimated uncertainties of the AIM measurements were approximately less than  
133 15% (Trebs et al., 2004; Pathak et al., 2011). Some measures were taken out to reduce  
134 error, for instance, standards solutions were periodically injected to check the  
135 consistency of sensitivity of the detectors and air flow rate is frequently checked using  
136 a calibrated flow meter.

137 A semi-continuous OC/EC analyzer (Sunset Laboratory, Forest Grove, Oregon,  
138 USA) was applied to determine the carbonaceous species in PM<sub>2.5</sub>. This instrument  
139 used the thermal-optical transmittance method based on NIOSH Method 5040.  
140 Organic compounds were vaporized in pure helium and then oxidized to CO<sub>2</sub> in a  
141 manganese dioxide oxidizing oven. CO<sub>2</sub> was then quantified by non-dispersive  
142 infrared detector. EC was then desorbed in an oxygen blend carrier gas and then  
143 oxidized and quantified using the same method as for OC. The split point between the  
144 pyrolyzed carbon formed from the organic carbon during the heating and EC that was  
145 originally in the sample was determined by measuring the transmission of a laser  
146 beam through the filter. Known volume of methane was injected, oxidized and  
147 quantified as an internal standard. Good correlations were found between the data  
148 measured by this instrument and filter-based laboratory analyses (Bae et al., 2004).

149 Visibility was monitored using the Belfort Model 6000 Visibility Sensor (Belfort  
150 Instrument Corp., MD, US). Trace O<sub>3</sub>, SO<sub>2</sub>, NO-NO<sub>2</sub>-NO<sub>x</sub> and CO gases were  
151 obtained with a resolution of 1 h by applying online analyzers (Thermo Instruments,  
152 TEI 49i, 43i, 42i and 48i, respectively). Meteorological parameters were collected  
153 using Met Station One (Met One Corp., OR, US).

154

## 155 **2.2 Data analysis methods**

### 156 **2.2.1 Reconstruction of the light extinction coefficient**

157 The light extinction ( $b_{\text{ext}}$ ) which is the sum of light scattering by particle ( $b_{\text{s,p}}$ ),  
 158 absorption by particle ( $b_{\text{a,p}}$ ), scattering by gas ( $b_{\text{s,g}}$ ), and absorption by gas ( $b_{\text{a,g}}$ ), is  
 159 reconstructed according to the revised IMPROVE algorithm as following (Pitchford et  
 160 al., 2007):

$$\begin{aligned}
 161 \quad b_{\text{ext}} &= b_{\text{s,p}} + b_{\text{a,p}} + b_{\text{a,g}} + b_{\text{s,g}} \\
 162 \quad &\approx 2.2 \times f_{\text{s}}(\text{RH}) \times [\text{Small } (\text{NH}_4)_2\text{SO}_4] + 4.8 \times f_{\text{L}}(\text{RH}) \times [\text{Large } (\text{NH}_4)_2\text{SO}_4] \\
 163 \quad &+ 2.4 \times f_{\text{s}}(\text{RH}) \times [\text{Small } \text{NH}_4\text{NO}_3] + 5.1 \times f_{\text{L}}(\text{RH}) \times [\text{Large } \text{NH}_4\text{NO}_3] \\
 164 \quad &+ 2.8 \times [\text{Small OM}] + 6.1 \times [\text{Large OM}] \\
 165 \quad &+ 1 \times [\text{Fine Soil}] + 1.7 \times f_{\text{ss}}(\text{RH}) \times [\text{Sea Salt}] \\
 166 \quad &+ 0.6 \times [\text{Coarse Mass}] + 10 \times [\text{EC Mass}] \\
 167 \quad &+ 0.33 \times [\text{NO}_2 \text{ (ppb)}] + \text{Rayleigh Scattering} \quad (1)
 \end{aligned}$$

168 where  $f_{\text{s}}(\text{RH})$  and  $f_{\text{L}}(\text{RH})$  are the water growth factors for small- and large-sized  
 169 distribution of sulfate and nitrate, respectively, and  $f_{\text{ss}}(\text{RH})$  is the water growth factor  
 170 for sea salt. Water growth factors are adopted according to Pitchford et al. (Pitchford  
 171 et al., 2007). The constant numbers in the above equation are extinction efficiencies  
 172 for each chemical species under dry condition.  $(\text{NH}_4)_2\text{SO}_4$  mass is estimated as 1.38  
 173 times of  $\text{SO}_4^{2-}$  mass and  $\text{NH}_4\text{NO}_3$  mass 1.29 times of  $\text{NO}_3^-$  mass assuming that  $\text{SO}_4^{2-}$   
 174 and  $\text{NO}_3^-$  are fully neutralized by  $\text{NH}_4^+$  in the forms of  $(\text{NH}_4)_2\text{SO}_4$  and  $\text{NH}_4\text{NO}_3$ ,  
 175 respectively, according to the revised IMPROVE method. Organic matter (OM) is  
 176 estimated as 1.8 times of OC concentration to account for unmeasured fractions.

177 The concentrations of sulfate, nitrate, and OM are divided into small- and  
 178 large-sized fractions in this algorithm. The size modes are described by log-normal  
 179 mass size distributions with geometric mean diameter and geometric standard  
 180 deviations. Concentrations of sulfate, nitrate, and OM in the large- and small-mode  
 181 are estimated using the following equations (taking sulfate as an example):

$$182 \quad [\text{Large } (\text{NH}_4)_2\text{SO}_4] = [\text{Total } (\text{NH}_4)_2\text{SO}_4]^2/20, \text{ for } [\text{Total } (\text{NH}_4)_2\text{SO}_4] < 20 \mu\text{g m}^{-3} \quad (2)$$

$$183 \quad [\text{Large } (\text{NH}_4)_2\text{SO}_4] = [\text{Total } (\text{NH}_4)_2\text{SO}_4], \text{ for } [\text{Total } (\text{NH}_4)_2\text{SO}_4] > 20 \mu\text{g m}^{-3} \quad (3)$$

184  $[\text{Small } (\text{NH}_4)_2\text{SO}_4] = [\text{Total } (\text{NH}_4)_2\text{SO}_4] - [\text{Large } (\text{NH}_4)_2\text{SO}_4]$  (4)

185

### 186 **2.2.2 Air mass back trajectory**

187 To study the impact of local and regional sources on the aerosol pollution in Suzhou,  
188 48-h back trajectories starting at 100 m from the sampling site were calculated using  
189 the NOAA HYSPLIT model ([http://ready.arl.noaa.gov/HYSPLIT\\_traj.php](http://ready.arl.noaa.gov/HYSPLIT_traj.php)). The back  
190 trajectories were calculated four times per day at starting times of 04:00, 10:00, 16:00,  
191 and 22:00 UTC, i.e. 12:00, 18:00, 00:00, and 06:00 local times, respectively. The  
192 trajectory cluster analysis was based on the GIS-based software TrajStat (Wang et al.,  
193 2009).

194

### 195 **2.2.3 Potential source contribution function**

196 The potential source contribution function (PSCF) method is based on the results of  
197 HYSPLIT model and can be used to identify the regional sources. The zone of  
198 concern is divided into  $i \times j$  small equal grid cells. The PSCF value for the  $ij$ th grid  
199 cell is calculated as:  $\text{PSCF}_{ij} = m_{ij}/n_{ij}$ , where  $n_{ij}$  is designated as the number of  
200 trajectory segment endpoints that fall in the  $ij$ th cell and  $m_{ij}$  is defined as the number  
201 of trajectory endpoints with pollutants concentrations higher than an set criterion  
202 (Ashbaugh et al., 1985; Wang et al., 2009). In present study, the average  
203 concentrations were treated as the criterion (Hsu et al., 2003). The PSCF values were  
204 multiplied by a weighting function  $W_{ij}$  to reduce the effect of small values of  $n_{ij}$  and to  
205 better reflect the uncertainty in the values for the cells with small  $n_{ij}$  values. The  
206 weighting function  $W_{ij}$  is defined as follows (Polissar et al., 1999):

207 
$$W_{ij} = \begin{cases} 1.00, & 80 < n_{ij} \\ 0.70, & 20 < n_{ij} \leq 80 \\ 0.42, & 10 < n_{ij} \leq 20 \\ 0.05, & n_{ij} \leq 10 \end{cases}$$

208



209 The PSCF value can be interpreted as the conditional probability that air masses  
210 with pollutants concentration greater than the set criterion pass through the *ij*th cell  
211 during transport to the receptor site (Wang et al., 2009). That is, cells with high PSCF  
212 values are indicative of regions having high potential contributions to the pollution at  
213 the receptor site.

214

### 215 **3. Results and discussion**

#### 216 **3.1 General characteristics of haze events**

217 As illustrated in Fig. 2, the visibility varied from a few hundred meters to more than  
218 50 km with a minimum value of only 322 m on Jan. 15, 2013, which was  
219 accompanied by high RH (82%). During the 2-month observation period, there were a  
220 total of ten periods when visibility was below 10 km. Excluding the five periods  
221 accompanied by precipitation, the other five periods were identified as haze events  
222 and all of these events occurred in January 2013. During the haze occurrence, hourly  
223 concentrations of PM<sub>2.5</sub> often exceeded 150  $\mu\text{g m}^{-3}$ , with a maximum concentration of  
224 324  $\mu\text{g m}^{-3}$  observed on Jan. 14, 2013. These concentrations were generally higher  
225 than those in normal periods. The daily concentrations of PM<sub>2.5</sub> on haze days varied  
226 from 148 to 196  $\mu\text{g m}^{-3}$ , which were 1.97 to 2.61 times the Grade II criteria of the  
227 national ambient air quality standard (75  $\mu\text{g m}^{-3}$ ). These values were comparable to  
228 that observed in Nanjing where the average PM<sub>2.5</sub> was 175.6  $\mu\text{g m}^{-3}$ , but slightly  
229 higher than those in some other cities in YRD where mean values were generally  
230 lower than 147.3  $\mu\text{g m}^{-3}$  when haze occurred in Jan. 2013 (Wang et al., 2014a; Wang  
231 et al., 2014d). The aerosol pollution happened in northeast China such as in Beijing,  
232 Tianjin, and Shijiazhuang were much severer, for instance, the daily and hourly  
233 concentrations of PM<sub>2.5</sub> were up to 368  $\mu\text{g m}^{-3}$  and 462  $\mu\text{g m}^{-3}$  in Tianjin in January 9  
234 to 13, 2013, and the maximum hourly value of approximately 1000  $\mu\text{g m}^{-3}$  was  
235 recorded in Beijing and Shijiazhuang in Jan. 2013 (Ji et al., 2014; Han et al., 2014;  
236 Wang et al., 2015).

237        Approximately 40% of the time in January 2013 met haze weather criteria,  
238        whereas no haze appeared in December 2012. Low amount of rainfall in January  
239        might be one of the factors causing the long duration of haze. Relative humidity (RH)  
240        was reported to be an important contributor to the visibility reduction. In the present  
241        study, visibility decreased with increasing RH, e.g. when RH increased from 42% to  
242        78%, visibility decreased from 42 km at 2:00 p.m. on 17 January to 4 km at 7:00 a.m.  
243        on 19 January. Statistically, RH was relatively higher during haze occurrence than  
244        clear periods. Low wind speed, smaller than  $5 \text{ m s}^{-1}$ , was frequently observed during  
245        this winter. Furthermore, wind speed was mostly less than  $1 \text{ m s}^{-1}$  during the haze  
246        events, lower than those in Beijing (Yang et al., 2015). Besides, atmospheric pressure  
247        was also found to be relatively low during the haze occurrences. The stagnant air, due  
248        to low wind speed and pressure, was unfavorable for aerosol horizontal transport or  
249        vertical diffusion, and therefore resulted in aerosol accumulation. Therefore,  
250        unfavorable weather conditions (high RH, and low rainfall, wind speed and  
251        atmospheric pressure) were among the causes forming haze in January 2013 in  
252        Suzhou as well as in many other cities (Wang et al., 2014b; Wang et al., 2014c; Wang  
253        et al., 2014d; Han et al., 2014; Yang et al., 2015).

254        In order to get more insights of the haze formation in this region, three haze  
255        events, which occurred on Jan. 19, from Jan. 21 to 26, and on Jan. 30, respectively,  
256        were further discussed below. Generally, the meteorological parameters and aerosol  
257        pollution level were comparable during these three haze occurrences, except for the  
258        relatively lower RH and higher temperature in the third haze events.

259

## 260        **3.2 PM<sub>2.5</sub> chemical composition and light extinction**

### 261        **3.2.1 PM<sub>2.5</sub> chemical composition**

262        The temporal variations of the concentrations of water-soluble inorganic ions (WSIIs)  
263        are illustrated in Fig. 3. The mean concentration of WSIIIs (including four anions and

264 five cations) was  $48.8 \pm 24.6 \mu\text{g m}^{-3}$ , accounting for 40% of  $\text{PM}_{2.5}$  mass concentration,  
265 slightly lower than that in Beijing which was  $69.4 \pm 55.8 \mu\text{g m}^{-3}$  and accounted for  
266 43% of  $\text{PM}_{2.5}$  (Tao et al., 2015).  $\text{SO}_4^{2-}$  was the most abundant species in WSIs, with  
267 averaged value of  $21.1 \pm 13.5 \mu\text{g m}^{-3}$ , followed by  $\text{NH}_4^+$  ( $13.9 \pm 5.69 \mu\text{g m}^{-3}$ ) and  
268  $\text{NO}_3^-$  ( $10.7 \pm 6.75 \mu\text{g m}^{-3}$ ), accounting for 43%, 29% and 21% of WSIs, respectively.  
269 These secondary inorganic components in total constitute 93% of total WSIs, close to  
270 the result in Beijing (Gao et al., 2015; Tao et al., 2015). The rest of ions,  $\text{Na}^+$  ( $1.36 \pm$   
271  $0.43 \mu\text{g m}^{-3}$ ),  $\text{K}^+$  ( $0.85 \pm 0.45 \mu\text{g m}^{-3}$ ),  $\text{Cl}^-$  ( $0.54 \pm 1.28 \mu\text{g m}^{-3}$ ),  $\text{Ca}^{2+}$  ( $0.34 \pm 0.27 \mu\text{g}$   
272  $\text{m}^{-3}$ ),  $\text{F}^-$  ( $0.06 \pm 0.72 \mu\text{g m}^{-3}$ ),  $\text{Mg}^{2+}$  ( $0.05 \pm 0.07 \mu\text{g m}^{-3}$ ), each had minor contribution  
273 ( $< 3\%$ ) to WSIs.

274  $\text{NO}_3^-$  and  $\text{SO}_4^{2-}$  are mainly formed from the transformation of their respective  
275 gaseous precursor of  $\text{NO}_x$  and  $\text{SO}_2$  (Wang et al., 2005). The emission ratio of  $\text{NO}_x$  to  
276  $\text{SO}_2$  was 17.2–52.6 for motor vehicles and 0.527–0.804 for stationary sources in the  
277 Yangtze River Delta, which means that the emissions of  $\text{SO}_2$  from motor vehicles  
278 were much less than  $\text{NO}_x$ , but the emissions of  $\text{SO}_2$  from stationary sources such as  
279 power plants, industrial boilers and furnaces were relatively higher than  $\text{NO}_x$  (Fu et  
280 al., 2008). Thus, the mass ratio of  $\text{NO}_3^-/\text{SO}_4^{2-}$  could be used as an indicator of the  
281 relative importance of mobile and stationary sources of sulfur and nitrogen in the  
282 atmosphere (Arimoto et al., 1996). In the present study, the averaged ratios of  
283  $\text{NO}_3^-/\text{SO}_4^{2-}$  and  $\text{NO}_x/\text{SO}_2$  were 0.59 and 5.68, respectively, indicating that emissions  
284 from vehicles and stationary sources were both important in Suzhou. The ratio of  
285  $\text{NO}_3^-/\text{SO}_4^{2-}$  in this study was lower than that in Beijing, but higher than those in  
286 Shanghai (0.43), Qingdao (0.35), Taiwan (0.20), and Guiyang (0.13) (Wang et al.,  
287 2006; Yao et al., 2002; Hu et al., 2002a; Fang et al., 2002; Xiao and Liu, 2004).

288 The  $\text{NO}_3^-/\text{SO}_4^{2-}$  ratio was relatively higher for 20% worst visibility hours (0.58)  
289 than 20% best visibility hours (0.54), suggesting that vehicle emission might play an  
290 important role in haze pollution. This was in agreement with the result in Guangzhou,  
291 where the  $\text{NO}_3^-/\text{SO}_4^{2-}$  ratio was 1.02 under stagnation and 0.55 in normal days, but  
292 contrary to that in Beijing, where the ratio in haze days (0.89) was lower than in

293 normal days (0.96) (Tan et al., 2009; Wang et al., 2006). In present study, NO<sub>x</sub>  
294 concentration greatly exceeded that of SO<sub>2</sub> during haze period, coincided with the  
295 result in Guangzhou, but disagreed with that in Beijing (Tan et al., 2009). Previous  
296 studies have indicated that high NO<sub>x</sub> emission may reduce the formation of OH and  
297 H<sub>2</sub>O<sub>2</sub>, and further decrease the possibility of SO<sub>4</sub><sup>2-</sup> formation (Tan et al., 2009). Thus,  
298 the elevation of NO<sub>3</sub><sup>-</sup> concentration under worse visibility conditions was greater than  
299 that of SO<sub>4</sub><sup>2-</sup> in both Suzhou and Guangzhou. The ratios of (NO<sub>3</sub><sup>-</sup>/SO<sub>4</sub><sup>2-</sup>) to (NO<sub>x</sub>/SO<sub>2</sub>)  
300 were lower for worse visibility period, in accordance with that in Beijing, showing  
301 that the nitrate concentrations may be also greatly affected by the re-volatilization of  
302 NH<sub>4</sub>NO<sub>3</sub> (Tan et al., 2009).

303 The carbonaceous species, constituting 22% of PM<sub>2.5</sub>, were dominated by  
304 organic carbon, which was  $22.8 \pm 10.6 \mu\text{g m}^{-3}$  and 3 to 29 times of that of elemental  
305 carbon ( $2.79 \pm 2.58 \mu\text{g m}^{-3}$ ), similar to those in Beijing (Tao et al., 2015). The  
306 relatively high ratios of OC/EC ( $10.6 \pm 4.29$ ), which were higher than the ratios in  
307 Beijing ( $7.1 \pm 0.5$ ) and Jinan ( $7.15 \pm 1.78$ ), demonstrated the existence of secondary  
308 organic carbon (SOC) (Ji et al., 2014; Zhang et al., 2014). The concentrations of SOC  
309 were estimated by applying the EC tracer method, which has been widely used to  
310 estimate the secondary organic aerosol contribution to PM<sub>2.5</sub> concentrations (Castro et  
311 al., 1999; Yang et al., 2005). The minimum ratio of OC/EC was 3.09 in the present  
312 study. The estimated SOC was  $14.2 \pm 5.69 \mu\text{g m}^{-3}$ , contributing 65% on average to  
313 OC. The SOC/OC was higher than 0.5 during almost the whole sampling period  
314 except on Jan. 30 when the third haze event occurred. This ratio was higher than most  
315 of the results found in other areas such as in Beijing and Guangzhou (Yang et al.,  
316 2005; Tan et al., 2009).

317 Major components in PM<sub>2.5</sub> were found to be SO<sub>4</sub><sup>2-</sup> (17%), SOC (14%), NH<sub>4</sub><sup>+</sup>  
318 (12%), NO<sub>3</sub><sup>-</sup> (8%), and POC (6%). The top four components were mainly from  
319 secondary sources. PM<sub>2.5</sub> was significantly correlated with these secondary species,  
320 revealing that gas to particle conversion was severe in winter and had great impact on  
321 aerosol pollution in this region. It's worth noting that the aerosol composition in the

322 third haze event was distinct from the other two (Fig. 3) as seen from the higher  
323 proportion of carbon species from primary emissions (POC and EC) and lower  
324 fraction of secondary formation components (SIA and SOC), indicating different haze  
325 formation mechanism in the third haze event.

326

### 327 **3.2.2 Light extinction coefficient**

328 In order to determine the contribution of PM<sub>2.5</sub> constituents to the visibility  
329 degradation, light extinction ( $b_{\text{ext}}$ ) was reconstructed based on the revised IMPROVE  
330 algorithm. In the present study, the impact of fine soil and coarse mass were not  
331 included because of the lack of metal elements and coarse matter concentrations. The  
332 estimated  $b_{\text{ext}}$  was  $664 \pm 288 \text{ Mm}^{-1}$  and was significantly correlated with PM<sub>2.5</sub>  
333 concentrations ( $r = 0.94$ ,  $p < 0.001$ ), demonstrating the strong influence of fine  
334 aerosols on visibility degradation.

335 The reconstructed light extinction coefficient was compared with that derived  
336 from visibility and that calculated using a regression model developed by Chen.  
337 Extinction coefficient is inversely correlated with visibility according to the  
338 Koschmieder equation ( $\text{Vis} = K/b_{\text{ext}}$ ) (Seinfeld and Pandis, 2012). By using a  $K$  value  
339 of 3.912, the calculated  $b_{\text{ext}}$  was  $371 \pm 234 \text{ Mm}^{-1}$ , much lower than the coefficients  
340 obtained from IMPROVE algorithm. Nevertheless, they were significantly correlated  
341 with each other ( $r = 0.71$ ,  $p < 0.001$ ). Another method applied here to estimate  $b_{\text{ext}}$   
342 was a 2-factor parameterization regression model based on RH and aerosol volume  
343 concentration (Chen et al., 2012). The volume concentration can be acquired from the  
344 mass concentration divided by an average particle density of  $1.7 \text{ g cm}^{-3}$  (Wehner et al.,  
345 2008). A comparison of  $b_{\text{ext}}$  reconstructed by IMPROVE algorithm and the regression  
346 model is presented in Fig. 4. Generally, a strong correlation was evident with a  
347 correlation coefficient higher than 0.97 ( $R^2 = 0.952$ ), confirming that the reconstructed  
348  $b_{\text{ext}}$  from the IMPROVE algorithm was reliable. The majority of  $b_{\text{ext}}$  was clustered  
349 near the 1:1 line for  $b_{\text{ext}} < 500 \text{ Mm}^{-1}$ , with the corresponding RH mainly below 75%.

350 However, for  $b_{\text{ext}} > 500 \text{ Mm}^{-1}$ , the dispersion of  $b_{\text{ext}}$  gradually increased, and most of  
351 the corresponding RH was higher than 75%. There are two possibilities causing these  
352 deviations. The first one is the ignorance of the impact of particle size distribution on  
353 light extinction in the 2-factor parameterization model applied here, as the variation of  
354 aerosol mass or volume fractions of different size particles can influence  $b_{\text{ext}}$  value  
355 especially under high RH (Chen et al., 2012). The second one is from the  
356 uncertainties of in situ measurements since RH sensor may have large errors under  
357 high RH condition. The regression model result was directly controlled by the RH  
358 value, and the hygroscopic growth factor in the IMPROVE algorithm depends on RH.

359 The light extinction was mostly influenced by aerosol light scattering as the  
360 estimated  $b_{\text{s,p}}$  was  $609 \pm 277 \text{ Mm}^{-1}$ , accounting for 91% of  $b_{\text{ext}}$ , while  $b_{\text{a,p}}$  and the  
361 extinction coefficient by gaseous were only  $27.9 \pm 25.8 \text{ Mm}^{-1}$  and  $26.6 \pm 4.87 \text{ Mm}^{-1}$ ,  
362 respectively. The largest contributor to  $b_{\text{ext}}$  from the reconstructed chemical species in  
363 fine particles was organic matter (OM), accounting for 40%, followed by  $(\text{NH}_4)_2\text{SO}_4$ ,  
364 34%,  $\text{NH}_4\text{NO}_3$ , 16%, and EC, 4%. However, the percentage contributor varied greatly  
365 during the study period, e.g. the contributions of  $\text{NH}_4\text{NO}_3$  ranged from only 3% to up  
366 to 40%. Generally, the contributions of  $(\text{NH}_4)_2\text{SO}_4$  and  $\text{NH}_4\text{NO}_3$  were higher under  
367 low visibility period, increased from 30% and 11%, respectively, during the 20% best  
368 visibility periods to 39% and 19%, respectively, during the 20% worst visibility  
369 period. Correspondingly, the contributions of OM and EC reduced from 46% and 5%,  
370 respectively, to 35% and 4%, respectively, during the same periods. These results  
371 indicated the important role sulfate and nitrate played on haze formation.

372 The percentage contribution to light extinction from individual aerosol  
373 components also varied with haze event and visibility conditions. The percentage  
374 contributions of individual components during the best and worst 20% visibility hours  
375 in each of the three haze events are compared and shown in Fig. 5. During the first  
376 haze event (on Jan. 19), the contribution of  $\text{NH}_4\text{NO}_3$  was 8% and 24% during the 20%  
377 best and worst visibility hours, respectively, while the corresponding numbers are  
378 48% and 37% for OM. There were no significant differences between the two

379 visibility categories for the contributions of  $(\text{NH}_4)_2\text{SO}_4$  or EC. During the second haze  
380 event (from Jan. 21 to 26), the fractions were 1.8, 1.5 and 1.3 times higher for  
381  $\text{NH}_4\text{NO}_3$ ,  $(\text{NH}_4)_2\text{SO}_4$  and EC respectively but 1.2 times lower for OM under 20%  
382 worst visibility condition than those under 20% best visibility condition during this  
383 time. Overall,  $(\text{NH}_4)_2\text{SO}_4$  made great contribution to the light extinction and  $\text{NH}_4\text{NO}_3$   
384 had largest difference between 20% best and worst visibility conditions during these  
385 two haze events. Therefore, secondary inorganic aerosols especially  $\text{NH}_4\text{NO}_3$  was  
386 likely the key component for the impaired visibility for these two haze events. The  
387 elevated proportion of  $(\text{NH}_4)_2\text{SO}_4$  and  $\text{NH}_4\text{NO}_3$  during the heavy polluted period was  
388 also observed in Beijing (Tao et al., 2015; Wang et al., 2015; Zheng et al., 2015). A  
389 different trend of comparison between the best and worst visibility periods was found  
390 in the third haze event (on Jan. 30) than in the first two. In the third event, the  
391 percentage contributions of OM and EC increased during the worst visibility period  
392 compared to the best visibility period (from 40% to 49% and 6.8% to 11%,  
393 respectively), while that of  $(\text{NH}_4)_2\text{SO}_4$  decreased (from 28% to 19%). Carbonaceous  
394 components played a more important role for visibility reduction in the third event.  
395 Therefore, there seems to be different formation mechanisms for haze events in  
396 Suzhou.

397

### 398 **3.3 Conversion from gas to particle phase**

#### 399 **3.3.1 Variations of aerosol particles and precursors**

400 Fig. 6 diagrammed the diurnal variations of meteorological parameters, various  
401 aerosol components, gaseous precursors, and some other important gaseous species  
402 under three different visibility conditions: (1) all data, (2) visibility  $\leq 10$  km, and (3)  
403 visibility  $> 10$  km. The daily variations of gas-phase compounds were different  
404 between species and were mainly controlled by the direct surface emissions (such as  
405  $\text{NO}_x$ ,  $\text{SO}_2$ , and CO) or photochemical process ( $\text{O}_3$ ). There were a distinct morning  
406 peak and a less distinct afternoon peak, consistent with morning and afternoon rush

407 hours for NO<sub>x</sub> and CO. This might be related to the heavy traffic emissions in the  
408 rush hours and the strong elevation of the Planetary Boundary Layer heights at noon.  
409 In contrast, there was only one mid-day peak for SO<sub>2</sub>. This diurnal profiles were  
410 similar to those observed in Guangzhou (Hu et al., 2002b) and Maryland (Antony  
411 Chen et al., 2001). In the latter study, the dominant source of SO<sub>2</sub> was considered to  
412 be the long range transport from the industrialized Midwest and with the deep  
413 boundary layer around noon; SO<sub>2</sub> aloft mixed more effectively down to the surface  
414 and thus caused the mid-day peak of SO<sub>2</sub>. The reasons for the diurnal variation of SO<sub>2</sub>  
415 observed in the present study need further investigation. Similar to the diurnal  
416 distribution of SO<sub>2</sub>, O<sub>3</sub> also showed one distinct peak around noon due to the strong  
417 photochemistry at that time (Quan et al., 2014).

418 For the aerosol components, EC which was also produced by the surface  
419 emissions showed a profile similar to NO<sub>x</sub> and CO. Furthermore, EC had  
420 significantly positive correlation with NO<sub>x</sub> and CO, demonstrating that they had  
421 common sources, mainly from vehicular exhaust. The diurnal profiles of the  
422 secondary species were similar to their precursors but obviously affected by other  
423 factors such as solar radiation, which could promote the oxidation of the precursors.  
424 For instance, there was a 2-hour delay for sulfate to reach its peak compared to SO<sub>2</sub>  
425 due to the transformation processes. This pattern was also observed in Guangzhou  
426 (Hu et al., 2002b). NO<sub>3</sub><sup>-</sup> and SOC exhibited similar diurnal variation as their  
427 precursors had common sources and they both formed from secondary photochemical  
428 oxidation. The daily profiles of NO<sub>3</sub><sup>-</sup>, NH<sub>4</sub><sup>+</sup> and SOC showed lower concentrations  
429 around 15:00 (local time) probably due to the high boundary layer and/or low  
430 concentration of precursors. Besides, for NO<sub>3</sub><sup>-</sup> and NH<sub>4</sub><sup>+</sup>, high temperature, which  
431 enhanced the evaporative loss, and low relative humidity may also be responsible for  
432 the low levels.

433 Fig. 6 also suggested that both gas-phase compounds and aerosol components all  
434 showed similar patterns of diurnal variations but had different magnitudes of  
435 concentrations for different visibility levels. These components except for O<sub>3</sub> all



436 showed relatively higher concentrations under low visibility especially for the  
437 secondary inorganic species, indicating the important impact of the formation of  
438 secondary components on the visibility reduction. The relatively low levels of O<sub>3</sub>  
439 under low visible conditions might be due to the decreased photochemical production  
440 and the chemical conversions of SO<sub>2</sub> and NO<sub>x</sub> to sulfate and nitrate. It is worth noting  
441 that the relatively high humidity which favored the formation of sulfate and nitrate  
442 was observed under low visibility conditions. In addition, it seemed that low visibility  
443 was associated with southwest wind. This might related to the topography. There are  
444 mountains located on the southwest which is not conducive to the diffusion of  
445 pollutants.

446 In consideration of the distinct aerosol composition during the third haze, the  
447 comparison of gaseous pollutants between the third and the first two haze episodes  
448 were made. The concentrations of SO<sub>2</sub> and O<sub>3</sub> were comparable for these three haze  
449 event. Contrarily, much higher levels of NO, CO and NO<sub>2</sub> were evident during the  
450 third haze, in accordance with the high concentrations of POC and EC. These species  
451 (NO, CO, NO<sub>2</sub>, POC and EC) had good correlations with each other. Furthermore,  
452 they had similar diurnal variations and exhibited extremely high levels in the morning  
453 rush hours on January 30 when the third haze occurred. These results implied that  
454 there were common sources for these species, mainly from vehicle exhaust emission.

455

### 456 **3.3.2 Formation mechanisms of sulfate and nitrate**

457 As discussed earlier, the chemical formation of sulfate and nitrate from SO<sub>2</sub> and NO<sub>2</sub>  
458 respectively, should play important roles for visibility reduction, especially for the  
459 first two haze events. The sulfur oxidation ratio, defined as  $SOR = n\text{-SO}_4^{2-} / (n\text{-SO}_4^{2-} +$   
460  $n\text{-SO}_2)$  and the nitrogen oxidation ratio, defined as  $NOR = n\text{-NO}_3^- / (n\text{-NO}_3^- + n\text{-NO}_2)$   
461 were used as indicators of the secondary transformation processes. The daily  
462 variations of NOR showed similar patterns as those of NH<sub>4</sub><sup>+</sup> and NO<sub>3</sub><sup>-</sup>. Likewise,  
463 SOR had similar diurnal changes as SO<sub>4</sub><sup>2-</sup>. The values of SOR and NOR increased

464 more than 1.3 and 2.0 times, respectively, during the first two haze periods compared  
465 to clear periods, implying greater oxidation of gaseous species and more elevated  
466 secondary aerosols. This was supported by the evidently higher concentrations of  
467  $\text{SO}_4^{2-}$ ,  $\text{NH}_4^+$ , and  $\text{NO}_3^-$  in the first two haze events. Almost no elevating levels of SOR,  
468 NOR or SIA were observed in the third haze, again confirming that the SIA formation  
469 may not be the predominant factor controlling the occurrence of this haze event.

470 The formation of  $\text{SO}_4^{2-}$  from  $\text{SO}_2$  was mainly ascribed to the gas-phase oxidation  
471 by OH and  $\text{H}_2\text{O}_2$  radical or heterogeneous oxidation (Wang et al., 2006; Zhao et al.,  
472 2013). The gas-phase reaction is a strong function of temperature and heterogeneous  
473 reactions always associated with high RH (Sun et al., 2006; Sun et al., 2014; Sun et al.,  
474 2013a). However, weak correlations were found between SOR and either temperature  
475 ( $r = 0.174$ ,  $p < 0.01$ ) or RH ( $r = 0.150$ ,  $p < 0.01$ ) in the present study, indicating the  
476 complex formation mechanism of sulfate.

477 Many studies suggested that sulfate from aqueous  $\text{SO}_2$  oxidation catalyzed by  
478 transition metals was more significant during winter haze rather than gas-phase  
479 oxidation (Li et al., 2011; Sun et al., 2013b; Zhao et al., 2013). Our measurement also  
480 found that the heterogeneous oxidation was an important sulfate formation pathway in  
481 this study area. As shown in Fig. 7, high concentrations of  $\text{NO}_2$  accompanied with  
482 ultralow level of  $\text{O}_3$  less than 10 ppb and low amount of solar radiation were observed  
483 during most of the time in the haze period, such as from 12 PM to 10 AM on 19  
484 January and from 21 to 34 January. These results revealed the rather weak  
485 photochemical activities during these time windows. The high levels of  $\text{NO}_2$  and  
486 weak photochemical activities could result in insufficient production of oxidants (OH  
487 and  $\text{H}_2\text{O}_2$  radicals) for gas-phase oxidation (Hua et al., 2008). Thus, other oxidation  
488 reactions other than gas-phase oxidation likely explained the formation of abundant  
489 secondary sulfates during the haze episode. The high RH ( $> 70\%$ ) during these haze  
490 period was a beneficial factor for aqueous-phase oxidation of  $\text{SO}_2$  to sulfate. Besides,  
491 the calculation results using the Extended AIM Aerosol Thermodynamic Model  
492 (E-AIM, Model II) (Clegg et al., 1998) (<http://www.aim.env.uea.ac.uk/aim/aim.php>)

493 showed a significant increase of the liquid water content when  $RH > 70\%$ . These  
494 results highlight the importance of aqueous-phase reaction to the secondary  
495 transformation of  $SO_2$ .

496 The concentrations of  $O_3$  were not extremely low during the whole haze period,  
497 such as during daytime on January 23 and 25; the  $O_3$  levels were as usual and had  
498 obvious diurnal variations with one distinct peak around noon.  $RH$  was lower than  
499 70% and sulfate was primarily in the solid phase at these times, indicating that  
500 gas-phase oxidation was probably the dominant pathway for sulfate formation.  
501 Aqueous-phase oxidation likely became predominant at night. This could explain the  
502 high SOR in the afternoon and the sustained high level at night.

503 Nitrate formation is mainly through gas-phase oxidation of  $NO_2$  by  $OH$  during  
504 daylight and the heterogeneous reactions of nitrate radical during nighttime (Seinfeld  
505 and Pandis, 2012). Fig. 8 showed the nitrate-to-sulfate molar ratio ( $[NO_3^-]/[SO_4^{2-}]$ ) as  
506 a function of the ammonium-to-sulfate molar ratio ( $[NH_4^+]/[SO_4^{2-}]$ ), which can  
507 provide an insight into the formation pathway of the secondary species (Jansen et al.,  
508 2014; Pathak et al., 2009; He et al., 2012). The relative abundance of nitrate linearly  
509 increased with the increasing ammonium-to-sulfate molar ratio. Fitting a linear  
510 regression line resulted in an intercept of  $[NH_4^+]/[SO_4^{2-}]$ -axis of 1.51, indicating that  
511 nitrate formation via homogeneous reaction of  $HNO_3$  with  $NH_3$  became significant at  
512  $[NH_4^+]/[SO_4^{2-}] > 1.51$  (Pathak et al., 2009; Jansen et al., 2014; He et al., 2012). Pathak  
513 et al. (2009) also reported an intercept value of 1.5 for several cities worldwide while  
514 Jansen et al. (2014) found a slightly smaller intercept value of 1.38 for Hangzhou. The  
515 ammonium concentration in excess of the amount at which nitrate formation became  
516 evident was defined as excess ammonium ( $[NH_4^+]_{exc} = ([NH_4^+]/[SO_4^{2-}] - 1.51) \times [SO_4^{2-}]$ ).  
517 The concentrations of excess ammonium were always higher than 0 and linearly  
518 correlated with nitrate concentration, as shown in Fig. 8. This indicated that the  
519 formation of nitrate was strongly associated with ammonium formation. In other  
520 words, when the excess ammonium was  $> 0$ , the gas-phase homogeneous reaction  
521 between the ambient ammonia and nitric acid was responsible for forming nitrate

522 (Pathak et al., 2009; Jansen et al., 2014). The slope of 0.37 for the regression and the  
523 scattering of the data indicated that the excess ammonium was bound to species other  
524 than nitrate, such as chloride, bisulfate, etc. The significance of gas-phase  
525 homogeneous reaction to nitrate formation has been reported for many cities (Jansen  
526 et al., 2014; Pathak et al., 2009). However, as mentioned above, in some cases during  
527 haze period, the conditions (ultralow ozone concentrations, low solar radiation and  
528 high NO<sub>2</sub>) were not favorable for the gas-phase oxidation. Relatively high RH were  
529 often observed in those cases, which may have favored the gas to particle partitioning  
530 of nitrate acid and ammonia (Sun et al., 2011). Furthermore, the E-AIM calculation  
531 results manifested that the nitrate partly or completely existed in the aqueous phase  
532 during those conditions. Therefore, we assumed that heterogeneous chemistry, such as  
533 heterogeneous hydrolysis of N<sub>2</sub>O<sub>5</sub> (N<sub>2</sub>O<sub>5</sub> + H<sub>2</sub>O (aq) → 2HNO<sub>3</sub>) or equilibrium  
534 partitioning (HNO<sub>3</sub> (g) + NH<sub>3</sub> (g) ↔ NH<sub>4</sub><sup>+</sup> (aq) + NO<sub>3</sub><sup>-</sup> (aq)) also contributed to the  
535 formation of nitrate under high RH conditions. This was supported by the fact that in  
536 Fig. 8 more plots were deviated from the regression line when RH were relatively  
537 high. The importance of heterogeneous reactions for nitrate formation were also  
538 reported in other studies (Sun et al., 2011; Zheng et al., 2015).

539

#### 540 **3.4 Regional sources deduced from trajectory and PSCF analyses**

541 The regional sources and transport of air pollutants exert a profound impact on local  
542 air quality in YRD region as it is located in the typical monsoon region (Ding et al.,  
543 2013). Therefore, trajectory clustering method was employed to examine the pathway  
544 of air masses and to look into the chemical composition and light extinction  
545 coefficients among the air masses with different origination. The calculated 48-h back  
546 trajectories were clustered into six clusters (Fig. 9 and Table 1), i.e. six air mass  
547 transport pathways. As can be seen, air masses reaching at Suzhou mainly came from  
548 local areas, the nearby provinces (cluster 2, accounting 31.7%), and the northwestern  
549 areas (cluster 1 and 3, both accounted for 20.6%).

550 High aerosol concentrations were associated with these trajectories. This was  
551 reasonable considering that these air masses passed over some highly industrialized  
552 cities, such as Hefei, Nanjing, and Hangzhou (Fig. 1). Relatively low levels of PM<sub>2.5</sub>  
553 were related to clusters 5 and 6. Based on the pathways and origins, these air masses  
554 were expected to bring in relatively clean air from the East China Sea and the Yellow  
555 Sea and consequently reduced the aerosol pollution in Suzhou.

556 Aerosols had high fractions of secondary inorganic ions (39%-42%) and  
557 relatively low contributions of OC (15%-16%) when the air masses fell in the C1, C3  
558 and C4, while had relatively high percentage of OC (36%) when the air masses fell  
559 into the C5. These differences of aerosol concentrations and composition in different  
560 clusters may result in distinct light extinction coefficients and species contributions to  
561 visibility reduction when air masses originated from different directions (Fig. 9).  
562 Similar to PM<sub>2.5</sub>, the reconstructed  $b_{\text{ext}}$  was the highest when air masses originated  
563 from the Northwest area (C3) and was relatively low when air masses fell into C5 and  
564 C6 areas. However, the lowest value of  $b_{\text{ext}}$  was in the C6 instead of C5 for the lowest  
565 PM<sub>2.5</sub> level, because of the higher contribution of OM in the C5. AS and OM were the  
566 dominant species determining the light extinction for all clusters. However, AS was  
567 the predominant contributor to light extinction for trajectories from north and  
568 northwest (C1, C3, C4), while in other cases the light extinction was primarily  
569 affected by OM. AN was the third highest contributor in all trajectory clusters with  
570 the largest contribution when air masses originated from northwest.

571 The origins of air masses in different haze events were further analyzed to  
572 interpret the relative contributions of chemical species to visibility reduction that  
573 differed between haze events. Most air masses fell into C1 and C3 (air masses from  
574 north and northwest, respectively) in the first two haze occurrence while all air mass  
575 trajectories were in C2 (air masses from local and nearby areas) for the third haze  
576 event. The contribution of OM to the total light extinction was higher in the third haze  
577 event than in the first two as discussed early, consistent with the results for cluster  
578 analysis that the light extinction was primarily impacted by AS for C1 and C3 but by

579 OM for C2. These results manifested that the third haze event was mainly contributed  
580 by the primary emission of carbon species from the local and/or surrounding areas.

581 It should be noted that air mass back trajectory analysis only suggests the  
582 originations and pathways of air masses but does not directly reveal the exact sources.  
583 Based on the results of trajectory analysis, the PSCF method was applied to explore  
584 the likely regional sources of major components in PM<sub>2.5</sub>, including sulfate, nitrate,  
585 OC, and EC, as illustrated in Fig. 10. Generally, PM<sub>2.5</sub> and the five aerosol species in  
586 Suzhou were mainly affected by local sources and nearby cities. Specifically, the  
587 higher value for PM<sub>2.5</sub> and the aerosol components were all localized in northwest to  
588 the south, covering surrounding cities in Jiangsu and near the border of Anhui and  
589 Zhejiang provinces. Additionally, these species were all affected by pollutions from  
590 Anhui province. Sulfate, nitrate and ammonium had similar spatial distributions, and  
591 relatively more affected by the north and northwest cities in Shandong, Jiangsu and  
592 Anhui provinces while pollutions from south cities in Zhejiang province had more  
593 impact on OC and EC in studied area than sulfate, nitrate and ammonium.

594

#### 595 **4. Conclusions**

596 Heavy aerosol pollution occurred in Suzhou in January 2013 with daily PM<sub>2.5</sub>  
597 concentrations on haze days 1.97 to 2.61 times higher than Grade II criteria of the  
598 national ambient air quality standard (75  $\mu\text{g m}^{-3}$ ) and maximum value of 324  $\mu\text{g m}^{-3}$   
599 on Jan. 14, 2013. Unfavorable weather conditions (high RH, low rainfall, wind speed  
600 and atmospheric pressure) especially high RH together with increased air pollutants  
601 produced from local and nearby sources were responsible for these haze formation.

602 During the first two haze periods, the major aerosol components were SO<sub>4</sub><sup>2-</sup>,  
603 NO<sub>3</sub><sup>-</sup>, NH<sub>4</sub><sup>+</sup>, and SOC, which were mainly from secondary sources. Furthermore,  
604 SOR and NOR both increased under worst visibility conditions, revealing efficient  
605 gas to particle conversion. Additionally, the contributions of (NH<sub>4</sub>)<sub>2</sub>SO<sub>4</sub> and NH<sub>4</sub>NO<sub>3</sub>  
606 to the reconstructed  $b_{\text{ext}}$  based on IMPROVE were higher under low visibility

607 conditions while those of OM and EC were higher under high visibility conditions,  
608 indicating that secondary inorganic aerosols especially  $\text{NH}_4\text{NO}_3$  seemed to be very  
609 important for the impaired visibility. Gas-phase homogeneous reaction might  
610 dominate the formation of sulfate and nitrate under low RH conditions while  
611 heterogeneous process might be responsible when RH were relatively high.

612 Distinctively, high proportion of carbon species from primary emission and  
613 lower fraction of secondary formation components were observed in the third haze.  
614 The SOR and NOR during the third haze episode were comparable to clean days.  
615 Moreover, increasing proportions of OM and EC accompanied with decreasing  
616 percentage of  $(\text{NH}_4)_2\text{SO}_4$  were found under worst visibility conditions when the third  
617 haze occurred. These results suggested that the carbon components from the primary  
618 emission might be relatively important for the visibility reduction for this haze event.

619 Trajectory clustering analysis showed that the air quality in Suzhou was mostly  
620 affected by air masses originating from North and Southwestern areas which were  
621 associated with high aerosol concentrations. Distinct aerosol composition profiles,  
622 light extinction coefficients and species contributions to visibility reduction were  
623 observed when air masses originated from different directions, e.g. AS was the  
624 predominant contributor to light extinction for trajectories from north and northwest,  
625 while in other cases the light extinction was primarily affected by OM.

626 The likely sources of aerosol and the major species based on the PSCF method  
627 were mainly from local anthropogenic activities and source emissions transported  
628 from nearby cities. The northwestern to southern regions may be important sources of  
629 aerosols and the major components. The northern and northwestern areas were  
630 predominant source regions for sulfate, nitrate and ammonium aerosols, whereas the  
631 southern area could be the common source region for carbonaceous species. This  
632 information has the implications for the importance of collaborative air pollution  
633 control strategy in the Yangtze River Delta Region.

634

635 **Acknowledgements**

636 This work was supported by the National Natural Science Foundation of China  
637 projects (41403089, 41375123), the "Strategic Priority Research Program" of the  
638 Chinese Academy of Sciences (KJZD-EW-TZ-G06-04), and the State Environmental  
639 Protection Key Laboratory of Sources and Control of Air Pollution Complex  
640 (SCAPC201310).

641



642 **References**

- 643 Antony Chen, L. W., Doddridge, B. G., Dickerson, R. R., Chow, J. C., Mueller, P. K.,  
644 Quinn, J., and Butler, W. A.: Seasonal variations in elemental carbon aerosol,  
645 carbon monoxide and sulfur dioxide: Implications for sources, *Geophys. Res. Lett.*,  
646 28, 1711-1714, doi: 10.1029/2000gl012354, 2001.
- 647 Arimoto, R., Duce, R. A., Savoie, D. L., Prospero, J. M., Talbot, R., Cullen, J. D.,  
648 Tomza, U., Lewis, N. F., and Jay, B. J.: Relationships among aerosol constituents  
649 from Asia and the North Pacific during PEM-West A, *J. Geophys. Res.-Atmos.*,  
650 101, 2011-2023, doi: 10.1029/95jd01071, 1996.
- 651 Ashbaugh, L. L., Malm, W. C., and Sadeh, W. Z.: A residence time probability  
652 analysis of sulfur concentrations at Grand-Canyon-National-Park, *Atmos. Environ.*,  
653 19, 1263-1270, doi: 10.1016/0004-6981(85)90256-2, 1985.
- 654 Bae, M.-S., Schauer, J. J., DeMinter, J. T., Turner, J. R., Smith, D., and Cary, R. A.:  
655 Validation of a semi-continuous instrument for elemental carbon and organic  
656 carbon using a thermal-optical method, *Atmos. Environ.*, 38, 2885-2893, doi:  
657 10.1016/j.atmosenv.2004.02.027, 2004.
- 658 Castro, L. M., Pio, C. A., Harrison, R. M., and Smith, D. J. T.: Carbonaceous aerosol  
659 in urban and rural European atmospheres: estimation of secondary organic carbon  
660 concentrations, *Atmos. Environ.*, 33, 2771-2781, doi:  
661 10.1016/S1352-2310(98)00331-8, 1999.
- 662 Charlson, R. J., Lovelock, J. E., Andreae, M. O., and Warren, S. G.: Oceanic  
663 phytoplankton, atmospheric sulfur, cloud albedo and climate, *Nature*, 326, 655-661,  
664 doi: 10.1038/326655a0, 1987.
- 665 Chen, J., Zhao, C. S., Ma, N., Liu, P. F., Göbel, T., Hallbauer, E., Deng, Z. Z., Ran, L.,  
666 Xu, W. Y., Liang, Z., Liu, H. J., Yan, P., Zhou, X. J., and Wiedensohler, A.: A  
667 parameterization of low visibilities for hazy days in the North China Plain, *Atmos.*  
668 *Chem. Phys.*, 12, 4935-4950, doi: 10.5194/acp-12-4935-2012, 2012.
- 669 Chen, R., Zhao, Z., and Kan, H.: Heavy smog and hospital visits in Beijing, China,  
670 *Am. J. Respir. Crit. Care Med.*, 188, 1170-1171, doi:

671 10.1164/rccm.201304-0678LE, 2013.

672 Chow, J. C., Doraiswamy, P., Watson, J. G., Antony-Chen, L. W., Ho, S. S. H., and  
673 Sodeman, D. A.: Advances in integrated and continuous measurements for particle  
674 mass and chemical, composition, *J. Air Waste Manage. Assoc.*, 58, 141-163, doi:  
675 10.3155/1047-3289.58.2.141, 2008.

676 Clegg, S. L., Brimblecombe, P., and Wexler, A. S.: Thermodynamic model of the  
677 system  $\text{H}^+ - \text{NH}_4^+ - \text{SO}_4^{2-} - \text{NO}_3^- - \text{H}_2\text{O}$  at tropospheric temperatures, *The Journal of*  
678 *Physical Chemistry A*, 102, 2137-2154, doi: 10.1021/jp973042r, 1998.

679 Ding, A. J., Fu, C. B., Yang, X. Q., Sun, J. N., Zheng, L. F., Xie, Y. N., Herrmann, E.,  
680 Nie, W., Petaja, T., Kerminen, V. M., and Kulmala, M.: Ozone and fine particle in  
681 the western Yangtze River Delta: an overview of 1 yr data at the SORPES station,  
682 *Atmos. Chem. Phys.*, 13, 5813-5830, doi: 10.5194/acp-13-5813-2013, 2013.

683 Fang, G. C., Chang, C. N., Wu, Y. S., Fu, P. P. C., Yang, C. J., Chen, C. D., and Chang,  
684 S. C.: Ambient suspended particulate matters and related chemical species study in  
685 central Taiwan, Taichung during 1998-2001, *Atmos. Environ.*, 36, 1921-1928, doi:  
686 10.1016/S1352-2310(02)00187-5, 2002.

687 Fu, Q., Zhuang, G., Wang, J., Xu, C., Huang, K., Li, J., Hou, B., Lu, T., and Streets, D.  
688 G.: Mechanism of formation of the heaviest pollution episode ever recorded in the  
689 Yangtze River Delta, China, *Atmos. Environ.*, 42, 2023-2036, doi:  
690 10.1016/j.atmosenv.2007.12.002, 2008.

691 Gao, J., Tian, H., Cheng, K., Lu, L., Zheng, M., Wang, S., Hao, J., Wang, K., Hua, S.,  
692 Zhu, C., and Wang, Y.: The variation of chemical characteristics of  $\text{PM}_{2.5}$  and  $\text{PM}_{10}$   
693 and formation causes during two haze pollution events in urban Beijing, China,  
694 *Atmos. Environ.*, 107, 1-8, doi: 10.1016/j.atmosenv.2015.02.022, 2015.

695 Han, S., Wu, J., Zhang, Y., Cai, Z., Feng, Y., Yao, Q., Li, X., Liu, Y., and Zhang, M.:  
696 Characteristics and formation mechanism of a winter haze-fog episode in Tianjin,  
697 China, *Atmos. Environ.*, 98, 323-330, doi: 10.1016/j.atmosenv.2014.08.078, 2014.

698 He, K., Zhao, Q., Ma, Y., Duan, F., Yang, F., Shi, Z., and Chen, G.: Spatial and  
699 seasonal variability of  $\text{PM}_{2.5}$  acidity at two Chinese megacities: insights into the  
700 formation of secondary inorganic aerosols, *Atmos. Chem. Phys.*, 12, 1377-1395,

701 doi: 10.5194/acp-12-1377-2012, 2012.

702 Hewitt, C. N.: The atmospheric chemistry of sulphur and nitrogen in power station  
703 plumes, *Atmos. Environ.*, *35*, 1155-1170, doi: 10.1016/S1352-2310(00)00463-5,  
704 2001.

705 Hsu, Y. K., Holsen, T. M., and Hopke, P. K.: Comparison of hybrid receptor models to  
706 locate PCB sources in Chicago, *Atmos. Environ.*, *37*, 545-562, doi:  
707 10.1016/S1352-2310(02)00886-5, 2003.

708 Hu, M., He, L. Y., Zhang, Y. H., Wang, M., Kim, Y. P., and Moon, K. C.: Seasonal  
709 variation of ionic species in fine particles at Qingdao, China, *Atmos. Environ.*, *36*,  
710 5853-5859, doi: 10.1016/S1352-2310(02)00581-2, 2002a.

711 Hu, M., Zhou, F., Shao, K., Zhang, Y., Tang, X., and Slanina, J.: Diurnal variations of  
712 aerosol chemical compositions and related gaseous pollutants in Beijing and  
713 Guangzhou, *J. Environ. Sci. Health A Tox. Hazard. Subst. Environ. Eng.*, *37*,  
714 479-488, doi: 10.1081/ese-120003229, 2002b.

715 Hua, W., Chen, Z. M., Jie, C. Y., Kondo, Y., Hofzumahaus, A., Takegawa, N., Chang,  
716 C. C., Lu, K. D., Miyazaki, Y., Kita, K., Wang, H. L., Zhang, Y. H., and Hu, M.:  
717 Atmospheric hydrogen peroxide and organic hydroperoxides during  
718 PRIDE-PRD'06, China: their concentration, formation mechanism and contribution  
719 to secondary aerosols, *Atmos. Chem. Phys.*, *8*, 6755-6773, doi:  
720 10.5194/acp-8-6755-2008, 2008.

721 Huang, R. J., Zhang, Y., Bozzetti, C., Ho, K. F., Cao, J. J., Han, Y., Daellenbach, K. R.,  
722 Slowik, J. G., Platt, S. M., Canonaco, F., Zotter, P., Wolf, R., Pieber, S. M., Bruns,  
723 E. A., Crippa, M., Ciarelli, G., Piazzalunga, A., Schwikowski, M., Abbaszade, G.,  
724 Schnelle-Kreis, J., Zimmermann, R., An, Z., Szidat, S., Baltensperger, U., El  
725 Haddad, I., and Prevot, A. S.: High secondary aerosol contribution to particulate  
726 pollution during haze events in China, *Nature*, *514*, 218-222, doi:  
727 10.1038/nature13774, 2014.

728 Jansen, R. C., Shi, Y., Chen, J., Hu, Y., Xu, C., Hong, S., Li, J., and Zhang, M.: Using  
729 hourly measurements to explore the role of secondary inorganic aerosol in PM<sub>2.5</sub>  
730 during haze and fog in Hangzhou, China, *Adv. Atmos. Sci.*, *31*, 1427-1434, doi:

731 10.1007/s00376-014-4042-2, 2014.

732 Ji, D., Li, L., Wang, Y., Zhang, J., Cheng, M., Sun, Y., Liu, Z., Wang, L., Tang, G., Hu,  
733 B., Chao, N., Wen, T., and Miao, H.: The heaviest particulate air-pollution episodes  
734 occurred in northern China in January, 2013: Insights gained from observation,  
735 *Atmos. Environ.*, 92, 546-556, doi: 10.1016/j.atmosenv.2014.04.048, 2014.

736 Khoder, M. I.: Atmospheric conversion of sulfur dioxide to particulate sulfate and  
737 nitrogen dioxide to particulate nitrate and gaseous nitric acid in an urban area,  
738 *Chemosphere*, 49, 675-684, doi: 10.1016/S0045-6535(02)00391-0, 2002.

739 Li, W., Zhou, S., Wang, X., Xu, Z., Yuan, C., Yu, Y., Zhang, Q., and Wang, W.:  
740 Integrated evaluation of aerosols from regional brown hazes over northern China in  
741 winter: Concentrations, sources, transformation, and mixing states, *J Geophys Res*,  
742 116, doi: 10.1029/2010jd015099, 2011.

743 Pathak, R. K., Wu, W. S., and Wang, T.: Summertime PM<sub>2.5</sub> ionic species in four  
744 major cities of China: nitrate formation in an ammonia-deficient atmosphere,  
745 *Atmos. Chem. Phys.*, 9, 1711-1722, doi: 10.5194/acp-9-1711-2009, 2009.

746 Pathak, R. K., Wang, T., and Wu, W. S.: Nighttime enhancement of PM<sub>2.5</sub> nitrate in  
747 ammonia-poor atmospheric conditions in Beijing and Shanghai: Plausible  
748 contributions of heterogeneous hydrolysis of N<sub>2</sub>O<sub>5</sub> and HNO<sub>3</sub> partitioning, *Atmos.*  
749 *Environ.*, 45, 1183-1191, doi: 10.1016/j.atmosenv.2010.09.003, 2011.

750 Pitchford, M., Maim, W., Schichtel, B., Kumar, N., Lowenthal, D., and Hand, J.:  
751 Revised algorithm for estimating light extinction from IMPROVE particle  
752 speciation data, *J. Air Waste Manage. Assoc.*, 57, 1326-1336, doi:  
753 10.3155/1047-3289.57.11.1326, 2007.

754 Polissar, A. V., Hopke, P. K., Paatero, P., Kaufmann, Y. J., Hall, D. K., Bodhaine, B.  
755 A., Dutton, E. G., and Harris, J. M.: The aerosol at Barrow, Alaska: long-term  
756 trends and source locations, *Atmos. Environ.*, 33, 2441-2458, doi:  
757 10.1016/S1352-2310(98)00423-3, 1999.

758 Quan, J., Tie, X., Zhang, Q., Liu, Q., Li, X., Gao, Y., and Zhao, D.: Characteristics of  
759 heavy aerosol pollution during the 2012–2013 winter in Beijing, China, *Atmos.*  
760 *Environ.*, 88, 83-89, doi: 10.1016/j.atmosenv.2014.01.058, 2014.

761 Ramanathan, V., and Vogelmann, A. M.: Greenhouse effect, atmospheric solar  
762 absorption and the Earth's radiation budget: From the Arrhenius-Langley era to the  
763 1990s, *Ambio*, 26, 38-46, 1997.

764 Seinfeld, J. H., and Pandis, S. N.: *Atmospheric Chemistry and Physics: From Air*  
765 *Pollution to Climate Change*, Second ed., John Wiley & Sons, Hoboken, New  
766 Jersey, 2012.

767 Sun, Y., Zhuang, G., Tang, A., Wang, Y., and An, Z.: Chemical Characteristics of  
768 PM<sub>2.5</sub> and PM<sub>10</sub> in Haze–Fog Episodes in Beijing, *Environ. Sci. Technol.*, 40,  
769 3148-3155, doi: 10.1021/es051533g, 2006.

770 Sun, Y., Jiang, Q., Wang, Z., Fu, P., Li, J., Yang, T., and Yin, Y.: Investigation of the  
771 sources and evolution processes of severe haze pollution in Beijing in January  
772 2013, *J. Geophys. Res.: Atmos.*, 119, 4380-4398, doi: 10.1002/2014jd021641,  
773 2014.

774 Sun, Y. L., Zhang, Q., Schwab, J. J., Chen, W. N., Bae, M. S., Lin, Y. C., Hung, H. M.,  
775 and Demerjian, K. L.: A case study of aerosol processing and evolution in summer  
776 in New York City, *Atmos. Chem. Phys.*, 11, 12737-12750, doi:  
777 10.5194/acp-11-12737-2011, 2011.

778 Sun, Y. L., Wang, Z. F., Fu, P. Q., Jiang, Q., Yang, T., Li, J., and Ge, X. L.: The impact  
779 of relative humidity on aerosol composition and evolution processes during  
780 wintertime in Beijing, China, *Atmos. Environ.*, 77, 927-934, doi:  
781 10.1016/j.atmosenv.2013.06.019, 2013a.

782 Sun, Y. L., Wang, Z. F., Fu, P. Q., Yang, T., Jiang, Q., Dong, H. B., Li, J., and Jia, J. J.:  
783 Aerosol composition, sources and processes during wintertime in Beijing, China,  
784 *Atmos. Chem. Phys.*, 13, 4577-4592, doi: 10.5194/acp-13-4577-2013, 2013b.

785 Tan, J., Duan, J., He, K., Ma, Y., Duan, F., Chen, Y., and Fu, J.: Chemical  
786 characteristics of PM<sub>2.5</sub> during a typical haze episode in Guangzhou, *J. Environ.*  
787 *Sci.*, 21, 774-781, doi: 10.1016/s1001-0742(08)62340-2, 2009.

788 Tao, J., Zhang, L. M., Ho, K. F., Zhang, R. J., Lin, Z. J., Zhang, Z. S., Lin, M., Cao, J.  
789 J., Liu, S. X., and Wang, G. H.: Impact of PM<sub>2.5</sub> chemical compositions on aerosol  
790 light scattering in Guangzhou - the largest megacity in South China, *Atmos. Res.*,

791 135, 48-58, doi: 10.1016/j.atmosres.2013.08.015, 2014.

792 Tao, J., Zhang, L., Gao, J., Wang, H., Chai, F., and Wang, S.: Aerosol chemical  
793 composition and light scattering during a winter season in Beijing, *Atmos. Environ.*,  
794 110, 36-44, doi: 10.1016/j.atmosenv.2015.03.037, 2015.

795 Tegen, I., Koch, D., Lacis, A. A., and Sato, M.: Trends in tropospheric aerosol loads  
796 and corresponding impact on direct radiative forcing between 1950 and 1990: A  
797 model study, *J. Geophys. Res.-Atmos.*, 105, 26971-26989, doi:  
798 10.1029/2000jd900280, 2000.

799 Tie, X., Madronich, S., Li, G., Ying, Z., Weinheimer, A., Apel, E., and Campos, T.:  
800 Simulation of Mexico City plumes during the MIRAGE-Mex field campaign using  
801 the WRF-Chem model, *Atmos. Chem. Phys.*, 9, 4621-4638, doi:  
802 10.5194/acp-9-4621-2009, 2009a.

803 Tie, X., Wu, D., and Brasseur, G.: Lung cancer mortality and exposure to atmospheric  
804 aerosol particles in Guangzhou, China, *Atmos. Environ.*, 43, 2375-2377, doi:  
805 10.1016/j.atmosenv.2009.01.036, 2009b.

806 Trebs, I., Meixner, F. X., Slanina, J., Otjes, R., Jongejan, P., and Andreae, M. O.:  
807 Real-time measurements of ammonia, acidic trace gases and water-soluble  
808 inorganic aerosol species at a rural site in the Amazon Basin, *Atmos. Chem. Phys.*,  
809 4, 967-987, doi: 10.5194/acp-4-967-2004, 2004.

810 Wang, H., An, J., Shen, L., Zhu, B., Pan, C., Liu, Z., Liu, X., Duan, Q., Liu, X., and  
811 Wang, Y.: Mechanism for the formation and microphysical characteristics of  
812 submicron aerosol during heavy haze pollution episode in the Yangtze River Delta,  
813 China, *Sci. Total Environ.*, 490, 501-508, doi: 10.1016/j.scitotenv.2014.05.009,  
814 2014a.

815 Wang, H., Xu, J., Zhang, M., Yang, Y., Shen, X., Wang, Y., Chen, D., and Guo, J.: A  
816 study of the meteorological causes of a prolonged and severe haze episode in  
817 January 2013 over central-eastern China, *Atmos. Environ.*, 98, 146-157, doi:  
818 10.1016/j.atmosenv.2014.08.053, 2014b.

819 Wang, J., Wang, S., Jiang, J., Ding, A., Zheng, M., Zhao, B., Wong, D. C., Zhou, W.,  
820 Zheng, G., Wang, L., Pleim, J. E., and Hao, J.: Impact of aerosol-meteorology

821 interactions on fine particle pollution during China's severe haze episode in  
822 January 2013, *Environ. Res. Lett.*, *9*, doi: 10.1088/1748-9326/9/9/094002, 2014c.

823 Wang, Y., Zhuang, G. S., Tang, A. H., Yuan, H., Sun, Y. L., Chen, S. A., and Zheng, A.  
824 H.: The ion chemistry and the source of PM<sub>2.5</sub> aerosol in Beijing, *Atmos. Environ.*,  
825 *39*, 3771-3784, doi: 10.1016/j.atmosenv.2005.03.013, 2005.

826 Wang, Y., Zhuang, G., Sun, Y., and An, Z.: The variation of characteristics and  
827 formation mechanisms of aerosols in dust, haze, and clear days in Beijing, *Atmos.*  
828 *Environ.*, *40*, 6579-6591, doi: 10.1016/j.atmosenv.2006.05.066, 2006.

829 Wang, Y., Yao, L., Wang, L., Liu, Z., Ji, D., Tang, G., Zhang, J., Sun, Y., Hu, B., and  
830 Xin, J.: Mechanism for the formation of the January 2013 heavy haze pollution  
831 episode over central and eastern China, *Sci. China-Earth Sci.*, *57*, 14-25, doi:  
832 10.1007/s11430-013-4773-4, 2014d.

833 Wang, Y. H., Liu, Z. R., Zhang, J. K., Hu, B., Ji, D. S., Yu, Y. C., and Wang, Y. S.:  
834 Aerosol physicochemical properties and implications for visibility during an  
835 intense haze episode during winter in Beijing, *Atmos. Chem. Phys.*, *15*, 3205-3215,  
836 doi: 10.5194/acp-15-3205-2015, 2015.

837 Wang, Y. Q., Zhang, X. Y., and Draxler, R. R.: TrajStat: GIS-based software that uses  
838 various trajectory statistical analysis methods to identify potential sources from  
839 long-term air pollution measurement data, *Environ. Modell. Softw.*, *24*, 938-939,  
840 doi: 10.1016/j.envsoft.2009.01.004, 2009.

841 Warneck, P.: *Chemistry of the natural atmosphere*, Academic press, 1999.

842 Wehner, B., Birmili, W., Ditas, F., Wu, Z., Hu, M., Liu, X., Mao, J., Sugimoto, N., and  
843 Wiedensohler, A.: Relationships between submicrometer particulate air pollution  
844 and air mass history in Beijing, China, 2004-2006, *Atmos. Chem. Phys.*, *8*,  
845 6155-6168, doi: 10.5194/acp-8-6155-2008, 2008.

846 Xiao, H. Y., and Liu, C. Q.: Chemical characteristics of water-soluble components in  
847 TSP over Guiyang, SW China, 2003, *Atmos. Environ.*, *38*, 6297-6306, doi:  
848 10.1016/j.atmosenv.2004.08.033, 2004.

849 Yang, F. M., He, K. B., Ma, Y. L., Zhang, Q., Cadle, S. H., Chan, T., and Mulawa, P.  
850 A.: Characterization of carbonaceous species of ambient PM<sub>2.5</sub> in Beijing, China, *J.*

851 Air Waste Manage. Assoc., 55, 984-992, doi: 10.1080/10473289.2005.10464699,  
852 2005.

853 Yang, Y., Liu, X., Qu, Y., Wang, J., An, J., Zhang, Y., and Zhang, F.: Formation  
854 mechanism of continuous extreme haze episodes in the megacity Beijing, China, in  
855 January 2013, *Atmos. Res.*, 155, 192-203, doi: 10.1016/j.atmosres.2014.11.023,  
856 2015.

857 Yao, X. H., Chan, C. K., Fang, M., Cadle, S., Chan, T., Mulawa, P., He, K. B., and Ye,  
858 B. M.: The water-soluble ionic composition of PM<sub>2.5</sub> in Shanghai and Beijing,  
859 China, *Atmos. Environ.*, 36, 4223-4234, doi: 10.1016/S1352-2310(02)00342-4,  
860 2002.

861 Yu, H. B., Liu, S. C., and Dickinson, R. E.: Radiative effects of aerosols on the  
862 evolution of the atmospheric boundary layer, *J. Geophys. Res.-Atmos.*, 107, AAC  
863 3-1–AAC 3-14, doi: 10.1029/2001jd000754, 2002.

864 Yu, S., Zhang, Q., Yan, R., Wang, S., Li, P., Chen, B., Liu, W., and Zhang, X.: Origin  
865 of air pollution during a weekly heavy haze episode in Hangzhou, China, *Environ.*  
866 *Chem. Lett.*, 12, 543-550, doi: 10.1007/s10311-014-0483-1, 2014.

867 Zhang, J., Chen, J., Yang, L., Sui, X., Yao, L., Zheng, L., Wen, L., Xu, C., and Wang,  
868 W.: Indoor PM<sub>2.5</sub> and its chemical composition during a heavy haze-fog episode at  
869 Jinan, China, *Atmos. Environ.*, 99, 641-649, doi: 10.1016/j.atmosenv.2014.10.026,  
870 2014.

871 Zhang, Q., Quan, J., Tie, X., Li, X., Liu, Q., Gao, Y., and Zhao, D.: Effects of  
872 meteorology and secondary particle formation on visibility during heavy haze  
873 events in Beijing, China, *Sci. Total Environ.*, 502, 578-584, doi:  
874 10.1016/j.scitotenv.2014.09.079, 2015.

875 Zhang, X. Y., Wang, Y. Q., Niu, T., Zhang, X. C., Gong, S. L., Zhang, Y. M., and Sun,  
876 J. Y.: Atmospheric aerosol compositions in China: spatial/temporal variability,  
877 chemical signature, regional haze distribution and comparisons with global  
878 aerosols, *Atmos. Chem. Phys.*, 12, 779-799, doi: 10.5194/acp-12-779-2012, 2012.

879 Zhao, X. J., Zhao, P. S., Xu, J., Meng, W., Pu, W. W., Dong, F., He, D., and Shi, Q. F.:  
880 Analysis of a winter regional haze event and its formation mechanism in the North



881 China Plain, *Atmos. Chem. Phys.*, 13, 5685-5696, doi: 10.5194/acp-13-5685-2013,  
882 2013.

883 Zheng, G. J., Duan, F. K., Su, H., Ma, Y. L., Cheng, Y., Zheng, B., Zhang, Q., Huang,  
884 T., Kimoto, T., Chang, D., Poeschl, U., Cheng, Y. F., and He, K. B.: Exploring the  
885 severe winter haze in Beijing: the impact of synoptic weather, regional transport  
886 and heterogeneous reactions, *Atmos. Chem. Phys.*, 15, 2969-2983, doi:  
887 10.5194/acp-15-2969-2015, 2015.

888

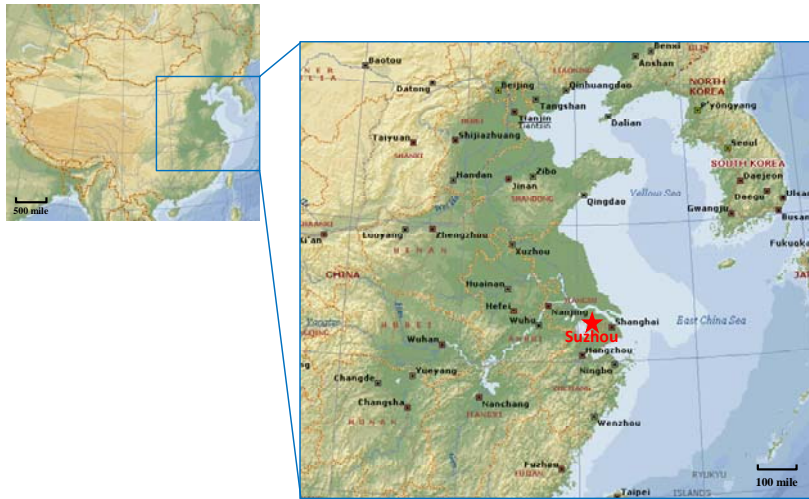
889

890 Table 1. The percentages of air masses from each trajectory cluster and associated  
 891 mean concentrations ( $\mu\text{g m}^{-3}$ ) of  $\text{PM}_{2.5}$  and its major chemical components, and mean  
 892  $b_{\text{ext}}$  ( $\text{Mm}^{-1}$ ).

	1	2	3	4	5	6
Percent (%)	20.6	31.7	20.6	12.7	6.3	7.9
$\text{PM}_{2.5}$	129	117	167	103	84.0	87.4
OC	21.1	22.8	25.3	16.4	30.5	20.3
EC	2.05	3.87	2.21	1.45	3.90	1.86
Sulfate	22.9	18.2	32.4	23.1	8.85	8.39
Nitrate	11.5	10.0	16.9	7.84	3.26	7.91
Ammonium	15.2	12.3	18.9	12.4	7.93	9.88
$b_{\text{ext}}$	675	597	921	556	548	463

893

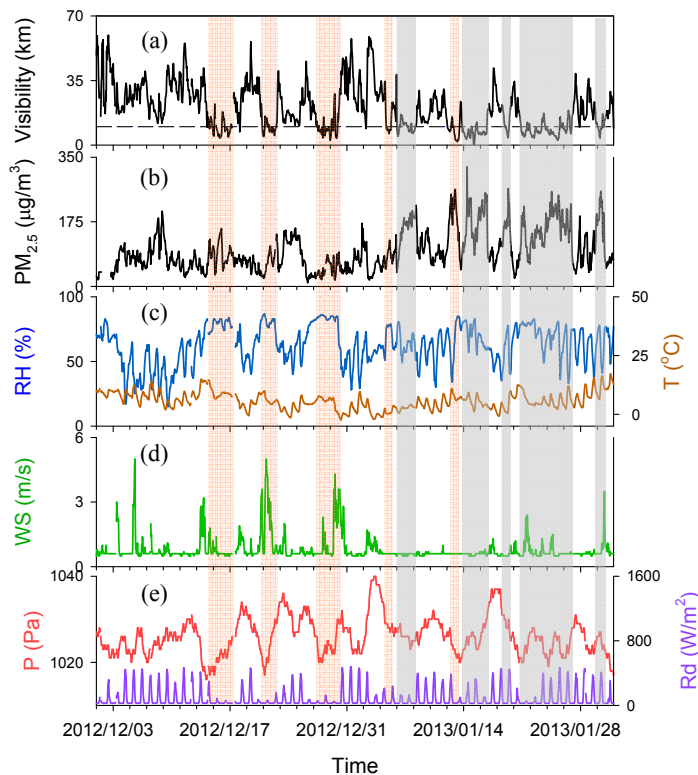
894



895

896 Figure 1. The sampling site in Suzhou. The locations of major cities with a population  
 897 of more than 1 million (such as Qingdao, Nanjing and Hangzhou) are marked with a  
 898 square symbol. The topographical map was derived from Microsoft® Encarta® 2009  
 899 © 1993 – 2008.

900

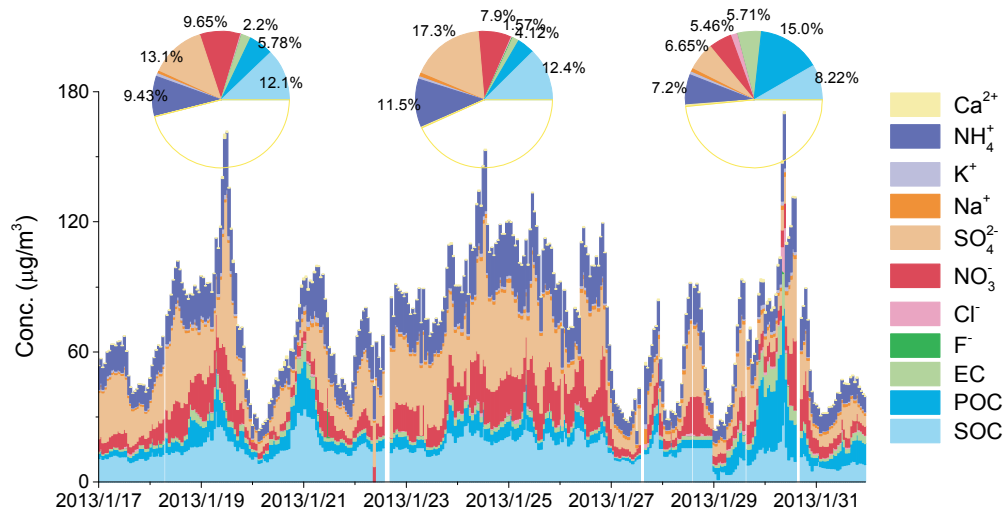


901

902 Figure 2. Time series of (a) visibility; (b)  $PM_{2.5}$  concentration; (c) relative humidity  
 903 (RH) and temperature (T); (d) wind speed (WS) and pressure (P); and (e) solar  
 904 radiation (Rd). The shaded areas in orange represent periods when visibility were

905 lower than 10 km and accompanied by precipitation. The shaded areas in grey  
 906 represent haze periods.

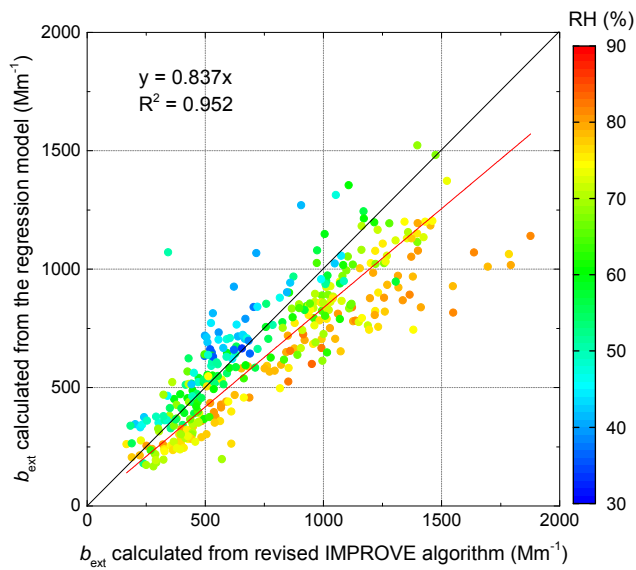
907



908

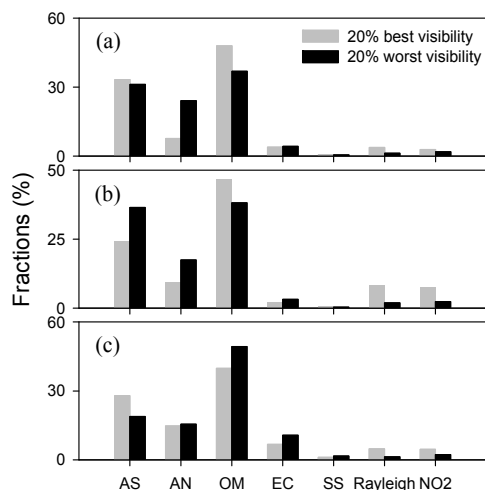
909 Figure 3. Temporal distribution of water soluble inorganic ions and carbonaceous  
 910 species. The aerosol composition in the three haze events was also illustrated in the  
 911 pie chart.

912



913

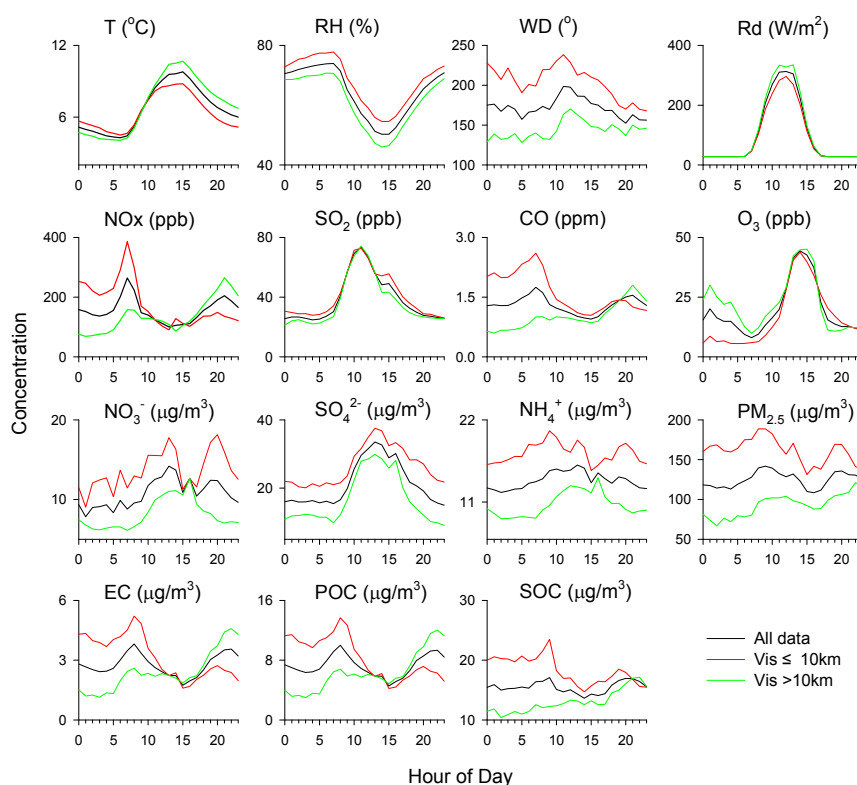
914 Figure 4. Comparison of the calculated  $b_{ext}$  between those obtained from the  
 915 regression equation and those from the IMPROVE algorithm.



916

917 Figure 5. Relative contributions of various chemical components in PM<sub>2.5</sub>  
 918 (ammonium sulfate (AS), ammonium nitrate (AN), OM, and EC) to the total light  
 919 extinction under 20% best and 20% worst visibility conditions during the first (a),  
 920 second (b), and third (c) haze events.

921

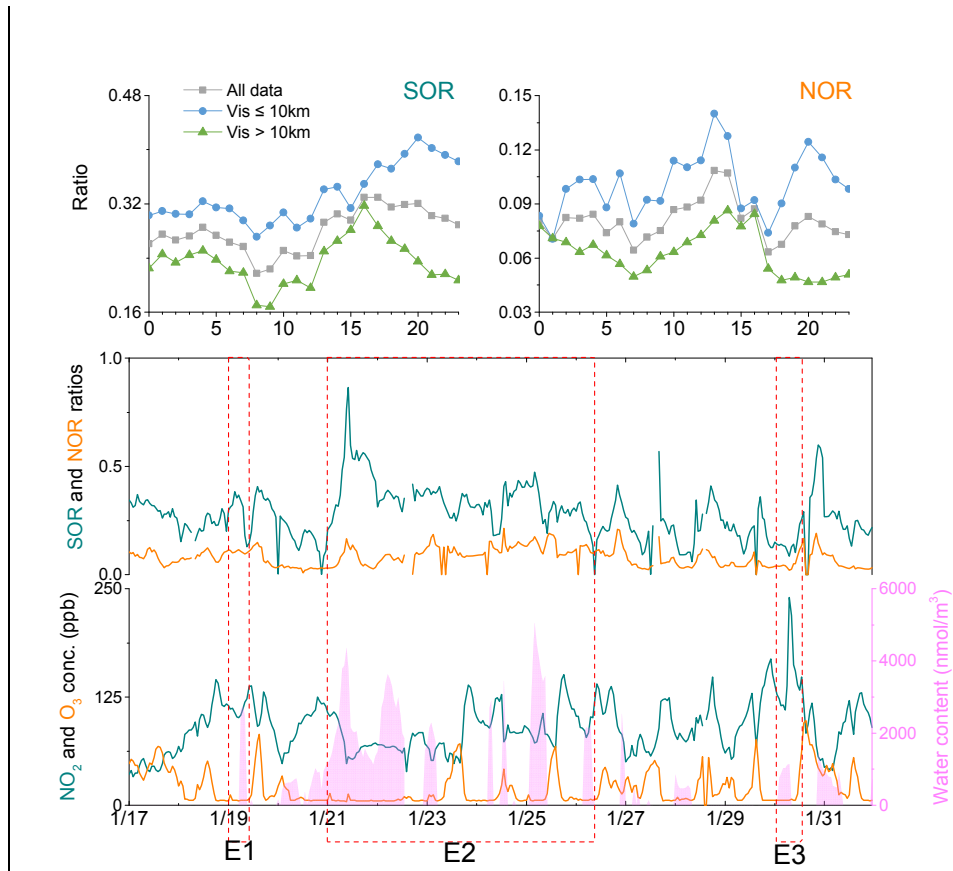


922

923 Figure 6. Diurnal profiles of meteorological variables, aerosol precursors (NO<sub>x</sub>, SO<sub>2</sub>),  
 924 CO, O<sub>3</sub>, PM<sub>2.5</sub>, and major aerosol compounds (NO<sub>3</sub><sup>-</sup>, SO<sub>4</sub><sup>2-</sup>, NH<sub>4</sub><sup>+</sup>, EC, POC, SOC)

925 under different visibility conditions.

926

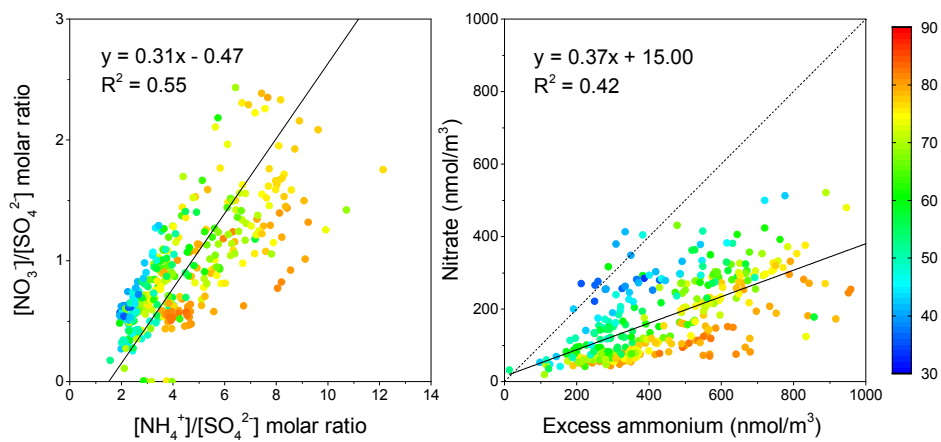


927

928 Figure 7. Temporary distributions of SOR, NOR, NO<sub>2</sub>, O<sub>3</sub> and aerosol water content.

929 Diurnal profiles of NOR and SOR ratios under different visibility conditions.

930



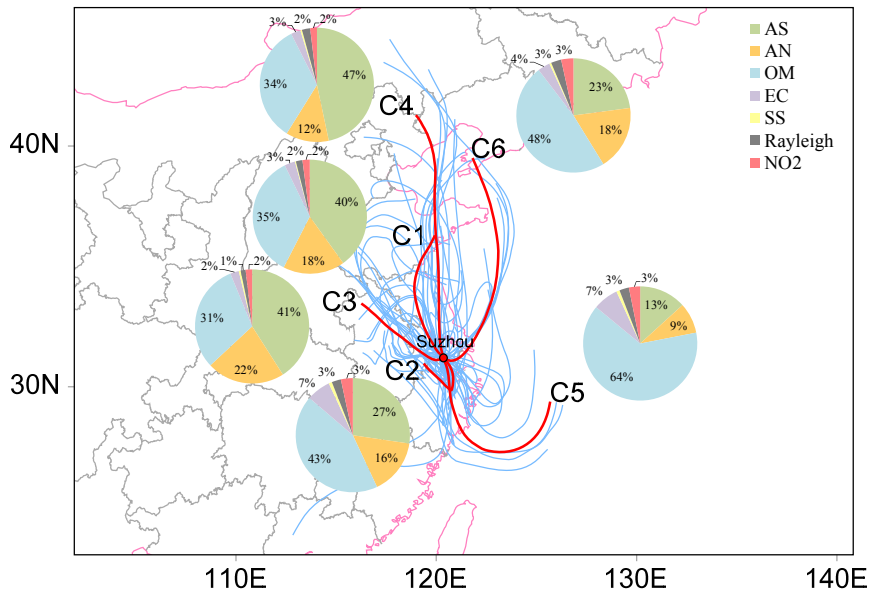
931

932 Figure 8. Nitrate to sulfate molar ratio as a function of ammonium to sulfate molar

933 ratio (left) and relationship between molar concentrations of nitrate and excess

934 ammonium (right).

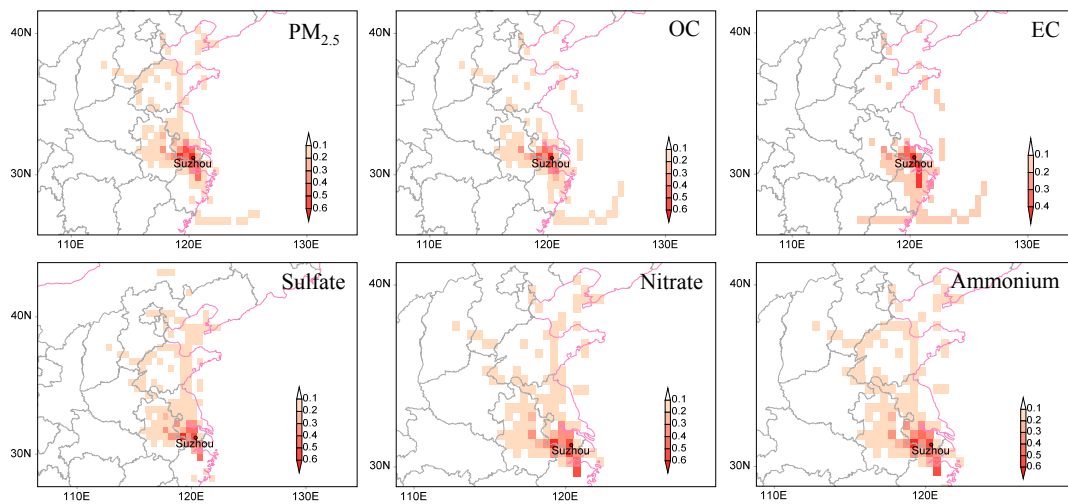
935



936

937 Figure 9. Backward air mass trajectories and six mean trajectories after the cluster  
938 analysis at the sampling site during Jan. 17 to 31. Relative contributions of various  
939 chemical components to the total light extinction in different clusters are illustrated.

940



941

942 Figure 10. The PSCF maps for PM<sub>2.5</sub>, OC, EC, sulfate, nitrate, and ammonium.

943